International Core Journal of Engineering Volume 10 Issue 6, 2024
ISSN: 2414-1895 DOI: 10.6919/ICJE.202406_10(6).0018

Application of Three-Dimensional Carbon Gel-based Catalysts in CO_2 Catalytic Conversion: A Review

Tongyu Bao*

School of Materials and Chemistry, University of Shanghai for Science and Technology, Shanghai 200093, China

*mrautumn001@gmail.com

Abstract

With the excessive consumption of fossil energy and the massive emission of CO_2, energy and environmental problems have become increasingly serious. The catalytic conversion of greenhouse gas CO_2 into high value-added fuels and chemicals is an ideal way to solve energy shortage and environmental pollution. Photocatalysis, electrocatalysis and thermal catalysis are commonly used strategies for catalytic conversion of CO_2. The problems of high recombination rate of carriers, catalyst agglomeration and difficult recovery of catalyst are widespread in various catalytic processes. Three-dimensional (3D) carbon gel have been applied in various types of catalytic reaction systems to solve above mentioned problems, due to their high conductivity, high specific surface area, high porosity, high CO_2 adsorption, rich resources and environmental friendliness. In this review, the theoretical basis of CO_2 catalytic conversion and the principles of photocatalysis, electrocatalysis and thermal catalysis of CO_2 will be introduced. Furthermore, we focus on the recent progress of 3D carbon gel-based catalysts in three types of CO_2 catalytic conversion systems. The future development opportunities and challenges of 3D carbon gel-based catalysts are also put forward.

Keywords

3D Carbon Gel; CO_2 Catalytic Conversion; Photocatalysis; Electrocatalysis; Thermal Catalysis.

1. Introduction

Excessive extraction and utilization of fossil fuels and increased emissions of greenhouse gas lead to increasingly serious energy and environmental issues, posing significant threats to both human society and the natural environment [1-7]. Greenhouse gases, especially CO_2, induce the greenhouse effect, precipitating global warming, substantial ice and snowmelt, and consequent sea-level rise. Various extreme climatic phenomena have become increasingly prevalent on a global scale, including events such as floods, droughts, marine storms, and extreme cold and heatwaves [8-13]. The catastrophic consequences resulting from these aberrant weather patterns severely constrain human societal activities and development [14-28]. The effectively prevent and control the threaten caused by the greenhouse effect is currently an urgent and important task globally. Extensive research has been conducted on the capture, utilization, and storage of CO_2 [29-35]. Carbon Capture and Storage (CCS) technologies were developed with the primary objective of minimizing the net emissions of the greenhouse gas CO_2 to the greatest extent possible [36-40]. In this regard, CO_2 capture technologies employ various separation and enrichment methods to obtain high-purity CO_2, such as physical/chemical adsorption, membrane separation, and cryogenic distillation [41-45]. Building

ISSN: 2414-1895 DOI: 10.6919/ICJE.202406_10(6).0018

upon carbon capture, subsequent carbon storage primarily encompasses terrestrial geological storage [46-52] and deep-sea sediment storage [53-56]. However, CCS technologies still confront numerous unresolved issues, such as the large-scale implementation of carbon capture and the risk of CO_2 leakage [57,58]. Compared to CCS technologies, the chemical conversion of CO_2 into high-value carbon-containing fuels (CO, CH_4, CH_3OH, etc.) and other valuable chemicals (such as urea) not only reduces the atmospheric concentration of CO_2 but also provides new energy, is a win-win carbon reduction path [59-64].

Various methods have been explored for catalytic reduction of CO_2, including photocatalysis [65-69], electrocatalysis [70-76], and thermocatalysis [77-79]. Despite significant developments have been made, there are still great challenges, such as the low sunlight utilization and high recombination rate of photogenerated charge carriers in photocatalysis, the competition reaction of hydrogen evolution reaction (HER) in electrocatalysis and the aggregation of catalysts in thermocatalysis. Simultaneously, a variety of challenges are commonly encountered in catalysis, such as poor catalytic stability, challenging catalyst recovery, weak CO_2 adsorption, and high costs. 3D carbon materials are expected to solve the above problems due to their unique physical, mechanical and electronic properties. This review presents recent development of 3D carbon gel-based composite catalysts, including carbon aerogels, graphene aerogels and graphene hydrogels, as well as their applications in photocatalysis, electrocatalysis and thermalcatalysis of CO_2 conversion.

2. Theoretical Foundations of CO_2 Catalytic Reduction

2.1 Physicochemical Properties of CO_2

CO_2 is a linear and centrally symmetric molecule. The length and bond energy of C=O bond is 116.3 pm and 799 kJ/mol, respectively. Although the C=O bond in CO_2 is polar, the dipole moment of the CO_2 molecule is zero due to its linear structure. CO_2 is chemically inert with low electron affinity and a significant energy gap (13.7 eV) between its lowest unoccupied molecular orbital (LUMO) and highest occupied molecular orbital (HOMO) [80]. Because of the highly oxidized state of carbon, CO_2 is thermodynamically stable ($\Delta_f G_{298}^{o}$ = -394.36 kJ/mol) [13]. Consequently, the conversion of CO_2 is an energetically uphill process, requiring a substantial input of energy [81,82]. Under standard conditions (1 atm, 298.15 K), the enthalpy change (ΔH^{o}) for the direct decomposition of CO_2 into CO and O_2 is 283.0 kJ/mol.

2.2 Adsorption and Activation of CO_2

The adsorption coordination of CO_2 molecules includes three modes: oxygen coordination, carbon coordination and mixed coordination [83]. For oxygen coordination, each O atom in CO_2 can donate lone pair electrons to the Lewis acid center on the adsorbent surface, which usually involves hydrogen bonding or electrostatic attraction. For carbon coordination, the C atom in CO_2 behaves as a Lewis acid, accepting electrons from Lewis base sites to form a carbonate-like structure; this coordination usually involves covalent bond formation. For mixed coordination, the interaction between the CO_2 molecule and the adsorbent surface involves both oxygen and carbon coordination, with the O and C atoms in CO_2 serving as electron donors and acceptors, respectively. The adsorption of CO_2 on the catalyst surface is typically accompanied by an activation process [84,85]. The activation of adsorbed CO_2 molecules is crucial for catalytic reduction of CO_2, which influences subsequent reduction processes and the extent of side reactions. At the catalyst surface, CO_2 molecules can interact with surface atoms, leading to a change in the electron distribution of the CO_2 molecules and the formation of partially charged $CO_2^{\delta-}$ species [86]. The $CO_2^{\delta-}$ species adsorbed on the catalyst surface determine the rate of CO_2 reduction and control product selectivity. The conversion of linear CO_2 molecules into bent anionic radicals $CO_2^{\delta-}$ requires additional energy for excitation to the high-energy state. Therefore, the energy barrier can be lowered by catalysts, which, in addition, can provide alternative reaction pathways to avoid the formation of high-energy intermediates.

ISSN: 2414-1895 DOI: 10.6919/ICJE.202406_10(6).0018

2.3 Reaction Pathways of CO_2 Reduction

The reduction of CO_2 is a complex redox reaction process, which involves the transfer of multiple electrons/protons, the breaking of C=O bonds and the formation of C-H bonds [4]. The process involves multiple types of intermediates, which depends on the reaction conditions, catalyst and mechanism [87,88]. Different reaction paths and types of intermediates generate different products, including mainly C_1 compounds (such as CO, CH_4, HCOOH, CH_3OH, HCHO, etc.) and C_2 compounds (such as C_2H_4, C_2H_5OH, CH_3COOH, etc.) [89]. Table 1 lists some half-reactions of CO_2 reduction in electrochemical reactions (ECR) and the corresponding reduction potentials (E^o) [90].

Table 1. The standard potentials (E^o) of possible half-reactions of electrochemical CO_2 reduction in aqueous solutions for the different hydrocarbon products at 25 °C, 1 atm, and pH 7 [90].

Possible Half-Reactions in ECR	E^o(V vs SHE)
$CO_2(g) + e^- \rightarrow CO_2^-$	−1.90
$CO_2(g) + 2H^+ + 2e^- \rightarrow HCOOH(l)$	−0.55
$CO_2(g) + 2H^+ + 2e^- \rightarrow CO(g) + H_2O(l)$	−0.52
$CO_2(g) + 4H^+ + 2e^- \rightarrow HCHO(l) + H_2O(l)$	−0.48
$CO_2(g) + 6H^+(l) + 6e^- \rightarrow CH_3OH(l) + H_2O(l)$	−0.38
$CO_2(g) + 8H^+ + 8e^- \rightarrow CH_4(g) + 2H_2O(l)$	−0.24
$2CO_2(g) + 12H^+ + 12e^- \rightarrow C_2H_4(g) + 4H_2O(l)$	−0.38
$2CO_2(g) + 12H^+ + 12e^- \rightarrow C_2H_5OH(l) + 3H_2O(l)$	−0.35
$2CO_2(g) + 14H^+ + 14e^- \rightarrow C_2H_6(l) + 4H_2O(l)$	−0.28
$3CO_2(g) + 18H^+ + 18e^- \rightarrow C_3H_7OH(l) + 5H_2O(l)$	−0.30

It can be concluded that efficient catalysts and sufficient energy input are essential conditions for the activation and reduction of CO_2 molecules during the catalytic reaction. Combining the catalyst with 3D carbon gel can effectively improve the catalytic performance (Figure 1) [91-93]. On the one hand, the 3D carbon gel has a high specific surface area, which increases the contact area between the catalyst and CO_2 molecules; on the other hand, the 3D carbon gel has a good adsorption of CO_2, which plays the role of CO_2 enrichment. The catalyst is uniformly dispersed on the 3D carbon gel in small size, which not only increases the number of reaction active sites, but also inhibits the agglomeration of the catalyst and improves the stability of the catalyst. Compared with powder catalysts, it is more convenient for recycling and reuse.

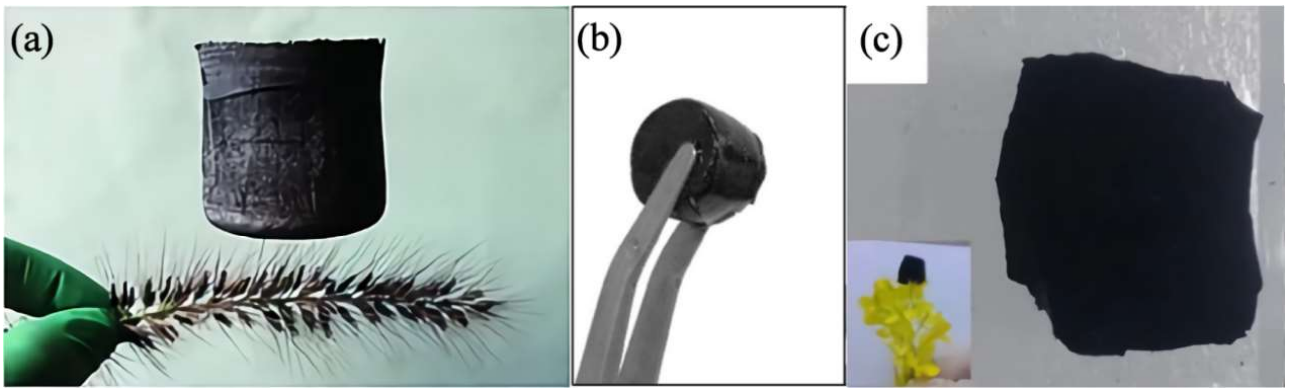

Figure 1. (a) Graphene aerogel[91]; (b) Graphene hydrogel[92]; (c) Carbon aerogel[93].

ISSN: 2414-1895 DOI: 10.6919/ICJE.202406_10(6).0018

3. Advancements in the Application of Three-Dimensional Carbon Gels in Catalytic CO_2 Reduction

3.1 Photocatalytic Reduction of CO_2

3.1.1 Principles of Photocatalytic Reduction of CO_2

The employment of solar-driven photocatalysis under mild conditions for the reduction of CO_2 holds significant promise. Semiconductor photocatalysts, activated by light radiation, engage photo-induced electrons in the reduction of CO_2, yielding high-value products [86]. The photocatalytic reduction of CO_2 primarily involves three sequential steps [94]: 1) Excitation via light absorption to generate electron-hole pairs; 2) Photogenerated charge carriers (electron-hole pairs) separation and migration to the photocatalyst's surface; 3) Subsequent photogenerated electron reduction of CO_2 and hole oxidation of redox agents at the photocatalyst's surface. During steps 2) and 3), electron-hole pairs may recombine, dissipating energy in the form of heat (non-radiative recombination) or light (radiative recombination), either within or at the surface of the photocatalyst, which is detrimental to the photocatalytic reduction of CO_2. Thus, only long-lived electrons and holes on the photocatalyst's surface possess the redox capability.

The preferred photocatalyst band gap is generally in the range of 1.75 to 3.0 eV, with strong absorption of visible light (about 43% of the solar spectrum), and should also have a high redox CO_2 potential.A suitable photocatalyst for CO_2 reduction needs to fulfill the following requirements: 1) A significant number of electrons should be easily captured by CO_2 molecules from the surface of the photocatalyst; 2) Its conduction band edge must be more negative than the reduction potential of CO_2 and its corresponding reduction products in electrochemistry; 3) CO_2 should be adsorbed on the photocatalyst, and product molecules should desorb and diffuse rapidly after reduction, avoiding photooxidation; 4) Photogenerated holes on the valence band of the photocatalyst should be consumed by a sacrificial agent, ideally generating gaseous O_2 through the oxidation of H_2O. Single semiconductor photocatalysts typically exhibit low photocatalytic efficiencies due to low solar energy capture capacity and poor carrier separation [95,96]. Therefore, efficient and stable composites are applied to overcome these limitations to improve the photocatalytic performance.

3.1.2 Application of Three-Dimensional Carbon Gels in Photocatalytic CO_2 Reduction

Given the inherent structural advantages and distinctive physicochemical properties of three-dimensional carbon gel materials, they play a significant role in enhancing the surface area and conductivity of photocatalysts and facilitating the separation of photogenerated charges. Jung et al.[97] fabricated TiO_2-graphene-MoS_2 (TGM) composite catalysts through a one-pot hydrothermal reaction, hybridizing TiO_2 nanoparticles, graphene aerogel (GA), and MoS_2 nanosheets (Figure 2a, b and c). Compared with the controls, TGM obtained the highest CO formation rate (92.33 μmol/(g·h)) (Figure 2d). The addition of GA provided carrier transfer channel, and the high conductivity of graphene facilitated charge transfer, effectively separating electron-hole pairs. Comparing the CO formation rates of TGM with different structures, TGM with macroporous 3D graphene and mesoporous TiO_2 obtained the CO formation rate ca. 3.4 times higher than that of TGM with non-3D graphene and mesoporous TiO_2 (nonmacro TGM) (Figure 2e). The 3D structure of GA not only inhibits the aggregation of the two-dimensional (2D) materials and provides more reaction sites and mass flow pathways, but also enhances the light absorption of the catalyst via multiple light reflections from the porous structure. In TGM, the photoinduced electrons were sequentially transferred through the TiO_2-graphene-MoS_2 (Figure 2f). Compared with 2D TiO_2-MoS_2, the photoinduced charges were transported stereographically in 3D graphene network, and the spatial separation for efficient carriers transfer increased the potential of oxidizing holes and reducing electrons, which significantly improved the charge transfer. In addition, the high concentration of electrons between the catalyst and graphene layers exceedingly improves the electronic conductivity of composites, which significantly enhances the co-catalytic activity of composites.

ISSN: 2414-1895 DOI: 10.6919/ICJE.202406_10(6).0018

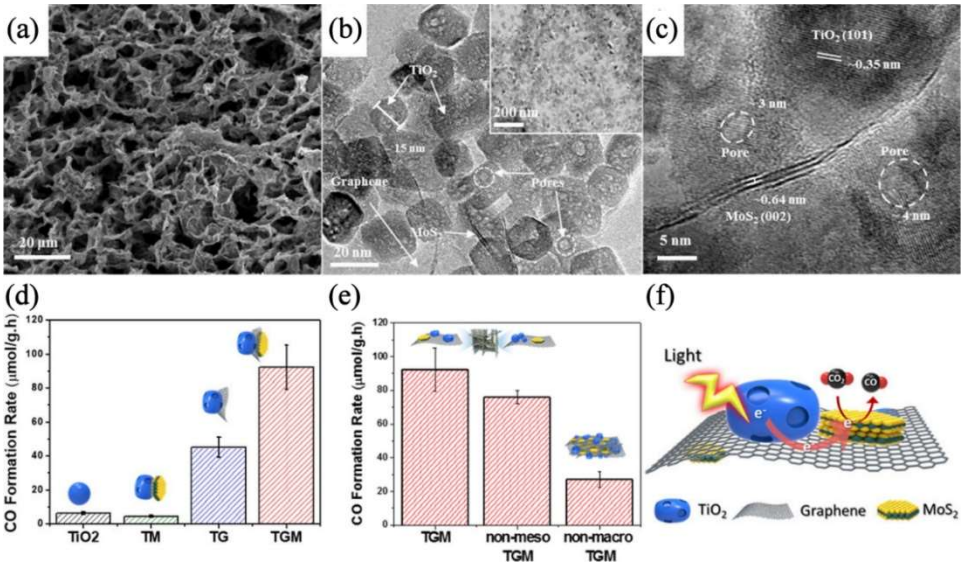

Figure 2. (a) SEM, (b) TEM and (c) HRTEM images of the TiO_2-graphene-MoS_2 (TGM) catalyst; (d) CO formation rates of TGM, TG, TM and TiO_2; (e) CO formation rates of TGM, nonmeso TGM and nonmacro TGM; (f) Possible CO_2 conversion mechanism of TGM[97].

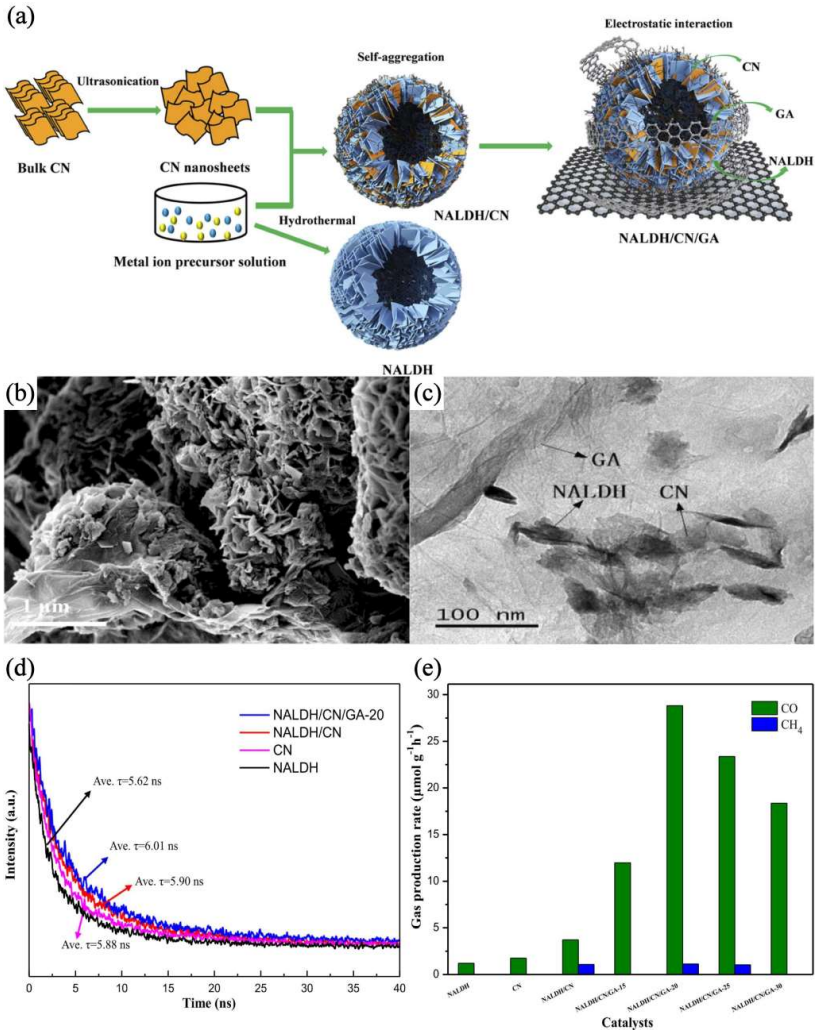

Figure 3. (a) Synthetic process for NALDH/CN/GA hybrid; (b) SEM and (c) TEM images of NALDH/CN/GA-20; (d) time-resolved fluorescence decay traces of the as-prepared samples; (e) CO and CH_4 average gas production rates over all synthesized photocatalysts[98].

ISSN: 2414-1895 DOI: 10.6919/ICJE.202406_10(6).0018

Yang et al.[98] prepared the hybrid heterojunction catalyst NALDH/CN/GA using a facile hydrothermal method by the compositing of NiAl layered double hydroxides (NiAl-LDH), g-C_3N_4 and graphene aerogel (Figure 3a). NALDH nanosheets and CN nanosheets form ultratight sheet-sheet heterojunctions in the presence of steric effect and hydrogen bonding. By introduction of GA, graphene was entwined with a curly folded layer structure, which enhanced the interfacial interaction between NALDH nanosheets and CN nanosheets (Figure 3b, and c). Compared with other samples, the average lifetime of the photogenerated charge carries in NALDH/CN/GA-20 is more prolonged (6.01 ns) (Figure 3d), and its CO yield rate reached 28.83 μmol/(g·h) (Figure 3e), which was 16 and 24 times those of pure CN and NALDH, respectively. The introduction of GA as an electronic medium and entwining agent, could furthermore promote charge transfer and coupling interface adhesion of heterojunctions, which enhance the separation of electron–hole pairs and mass transport, thus improving the photocatalytic performance.

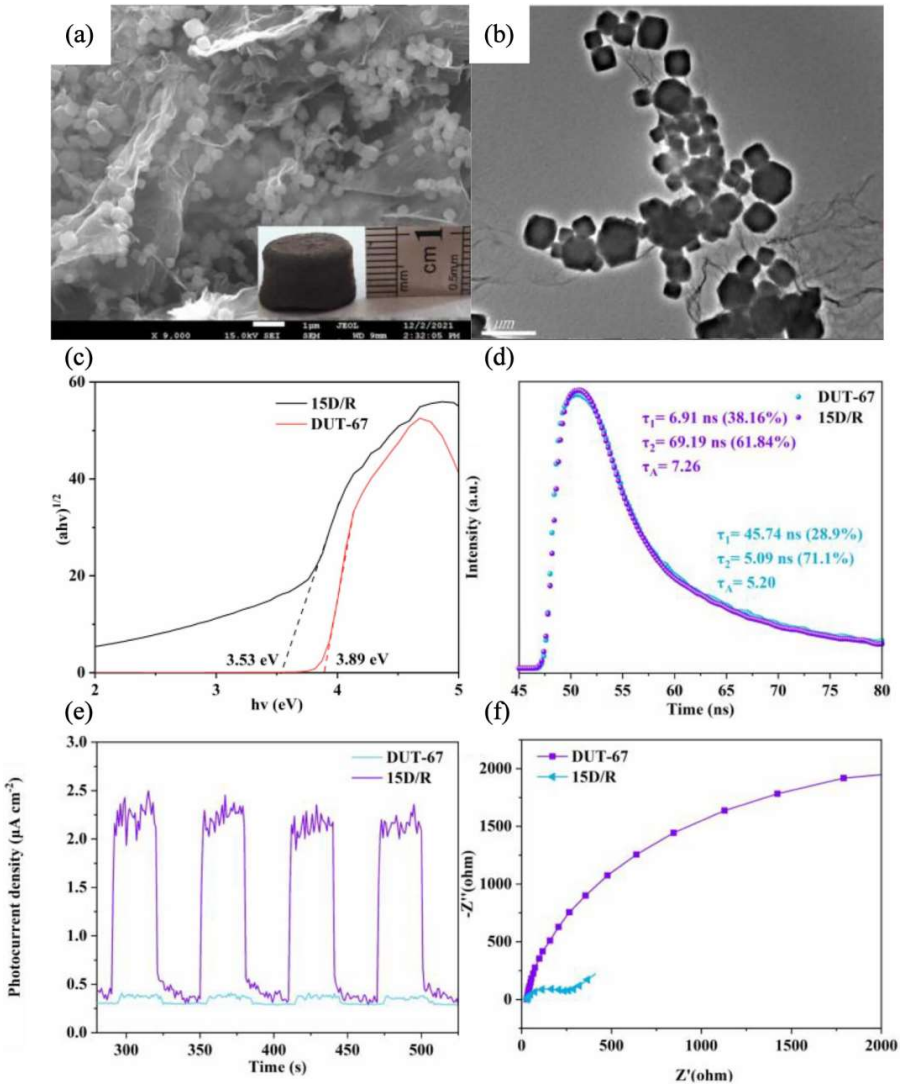

Figure 4. (a) SEM and (b) TEM images of 15D/R; (c) Tauc plots, (d) TRPL, (e) TPR and (f) EIS of DUT-67 and 15D/R[99]

Zhao et al.[99] constructed 3D DUT-67/RGO aerogel macrostructures through simple hydrothermal and freeze drying, based on Zr-based MOFs (DUT-67) and assisted by reduced graphene oxide (RGO) (Figure 4a and b). The multilayer structure of the 3D RGO aerogel dispersed DUT-67 uniformly in different sheets. Compared with pure DUT-67, the optimal ratio of 15DU-67/RGO aerogel (15D/R) had a narrower band gap (Figure 4c), which could more effectively absorb solar energy to generate

ISSN: 2414-1895 DOI: 10.6919/ICJE.202406_10(6).0018

electrons for photoreduction of CO_2. As a good electron acceptor, RGO prolonged the lifetime of photogenerated electrons through non-radiative quenching (Figure 4d), which increased the probability of photoelectrons participating in the photocatalytic reactions. The photocurrent density of 15D/R (2.21 μA/cm^2) was 5.9 times that of DUT-67 (0.37 μA/cm^2) (Figure 4e), and 15D/R also had the minimal charge transfer resistance (Figure 4f). 3D RGO aerogel had good electronic conductivity, which reduced the interface charge transfer resistance from DUT-67 to RGO and enhanced the photogenerated charge separation efficiency of DUT-67. In addition, it was confirmed that the synergistic effect of DUT-67 and RGO aerogel structure made 15D/R have strong adsorption/activation ability for CO_2.

In the above photocatalysis reports, the 3D graphene aerogel was introduced into the photocatalyst as a carrier, which could effectively reduce the interface charge transfer resistance and promote the photogenerated electron-hole pair separation due to its high conductivity and large specific surface area. The 3D network structure not only avoids the stacking caused by strong interactions between 2D graphene sheets but also improves the catalyst dispersion and inhibits the catalyst aggregation, which can provide more active sites for catalytic reactions. The highly interconnected porous structure provid a way for the adsorption and mass transfer of CO_2 and multiple reflections and absorption of incident light. It can be seen that the composites of photocatalysts with graphene aerogels can effectively address some of the issues in photocatalysis processes, further enhancing photocatalytic performance.

3.2 Electrocatalytic Reduction of CO_2

3.2.1 Principles of Electrocatalytic Reduction of CO_2

Electrocatalysis is the combination of electrochemistry and catalysis. Electrochemistry interconverts electrical and chemical energy, while catalysis reduces the activation energy of reactions and accelerates the rate of chemical reactions. Electrocatalysis is a special type of multiphase catalysis that involves interactions and electron exchange between reactants and electrocatalysts, and it utilizes currents to improve the rate and efficiency of chemical reactions. The electrocatalytic process encompasses cathodic and anodic reactions, driven by an external power source to facilitate non-spontaneous electron transfer reactions, thereby converting electrical energy into the chemical energy of the products. The composition of the cathode/anode in the process consists of the electron-conducting phase (electrode) connected by the ion-conducting phase (electrolyte). Electrocatalysts are typically used as electrodes or attached to the electrode surface, which can facilitate specific electrochemical conversions rapidly [100].

The CO_2 electrochemical reduction reaction (CO_2RR) occurs at the cathode electrode/electrolyte interface and consists of the following three main steps [101]: 1) CO_2 adsorption on the catalyst surface; 2) Proton and electron transfer; 3) Generation and diffusion of new products. The electrocatalytic interface structure is typically divided into five distinct regions, including the electrode surface, the inner Helmholtz plane (IHP), the outer Helmholtz plane (OHP), the diffusion layer and the bulk solution. The CO_2RR is an inner-sphere reaction process [102]. Adsorption and bond rearrangement of CO_2 molecules and reaction intermediates occur in the IHP [103]. As CO_2 molecules approach the electrode surface, they interact with the electrolyte and the electrode, resulting in proton and electron transfer.

An ideal CO_2RR catalyst should possess the following characteristics: 1) High voltage efficiency: promoting the reduction of CO_2 at lower potentials to enhance energy conversion efficiency; 2) High product selectivity: selectively converting CO_2 into the desired organic compounds or other products without generating unwanted byproducts; 3) Rapid kinetics: being capable of operating at high current densities to improve reaction rates and production rates; 4) Stability: exhibiting a long service life and good resistance to changes in feed gases and electrolytes, and common impurities that may be encountered. 3D carbon gels are carbon materials with outstanding properties, which are commonly used in electrocatalytic applications. The high surface area, conductivity, and porosity make them excellent catalyst support materials. 3D carbon gels can provide a large number of active sites,

ISSN: 2414-1895 DOI: 10.6919/ICJE.202406_10(6).0018

contributing to the enhancement of CO_2RR catalyst performance. Furthermore, their structural stability and corrosion resistance also make them promising materials for electrocatalytic reactions.

3.2.2 Application of Three-Dimensional Carbon Gels in Electrocatalytic CO_2 Reduction

Xiao et al.[104] prepared carbon aerogels (CA) loaded with copper nanoparticles (Cu NPs) using resorcinol and formaldehyde as RF resin precursors and copper acetate as catalyst. Further activation was explored under CO_2 and N_2 calcination. The optimal catalyst Cu/CA-CO_2-N_2-700 was obtained under the secondary N_2 atmosphere and activation temperature of 700 °C. CA has an abundant porous structure (Figure 5a). The in-situ formed Cu NPs were uniformly dispersed in the carbon network (Figure 5b). The interconnected structure of Cu NPs and CA existed synergistic effect, facilitating the enhanced catalytic activity. Cu/CA-CO_2-N_2-700 exhibited lower onset potential in CO_2 as compared to N_2, indicating its higher activity for CO_2 reduction (Figure 5c). CO_2RR activity was higher than HER activity and could highly suppress HER. Cu/CA-CO_2-N_2-700 had excellent stability and was able to maintain the metallic nature of Cu component within the carbon aerogels during electrocatalysis, achieving the high selectivity toward CO, with a Faradaic efficiency of 75.6% (Figure 5d). The contact angle of Cu/CA-CO_2-N_2-700 was 113°. The hydrophobicity and porous structure of CA could repel water but benefit the diffusion of CO_2 and CO (Figure 5e).

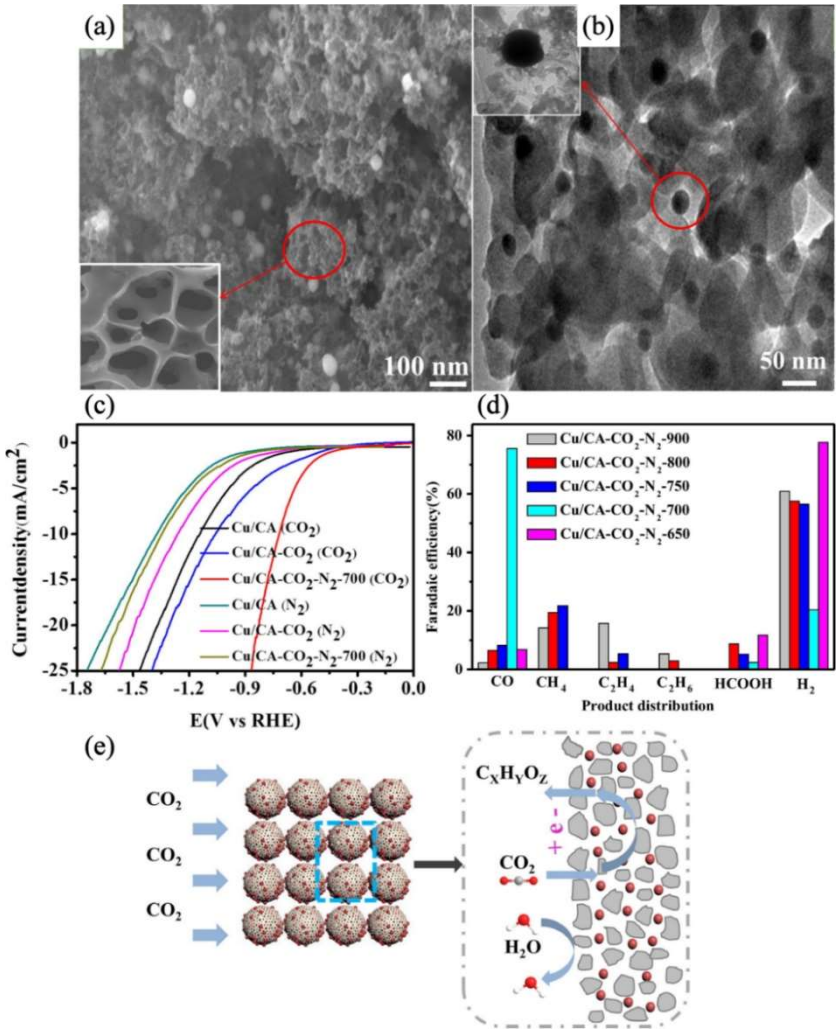

Figure 5. (a) SEM and (b) TEM images of Cu/Ac-CO_2-N_2-700; (c) LSV curves of Cu/CA, Cu/CA-CO_2 and Cu/CA-CO_2-N_2-700 on glassy carbon electrodes in N_2- or CO_2-saturated 0.1 M $KHCO_3$ aqueous solution; (d) Faradaic efficiency (-0.6V vs. RHE) of CO_2 electro-reduction products of Cu/CA-CO_2-N_2-T (T=650 ℃, 700 ℃, 750 ℃, 800 ℃ and 850 ℃); (e) Schematic of CO_2 electrochemical reduction under Cu/CA-CO_2-N_2-T[104].

ISSN: 2414-1895 DOI: 10.6919/ICJE.202406_10(6).0018

Mou et al.[105] employed melamine foam (MF) as a template for graphene oxide (GO) aerogel (GA) and loaded Ni single atoms (NiSA) onto GA by impregnation-pyrolysis method (Figure 6a). Graphene-based aerogels can not only inherit graphene's outstanding intrinsic properties but also possess large specific surface area and pore volume, which allows for the uniform dispersion of the electrocatalysts on the graphene sheet. (Figure 6b). GO exhibits numerous defects that can serve as "traps" to capture nickel precursors and anchor nickel atoms with aid of charge-transfer effect, achieving a high nickel loading of approximately 2.6 wt%. At electrolytic potentials of -0.8 V vs RHE, the highest CO Faradaic efficiency reached 90.2% (Figure 6c). GA utilized doped N, derived from MF, to anchor neighboring Ni^{2+} ions and prevent agglomeration of Ni atoms, which constructed Ni-N_x sites (Figure 6d). Comparing the Gibbs free energy of reaction pathway on different Ni-N_x sites, the free energy for the formation of *COOH on Ni-N_2 (0.17 eV) and Ni-N_3 (0.84 eV) are significantly lower than that on Ni-N_4 (1.34 eV) (Figure 6e). The high CO_2RR activity originates from the coordinatively unsaturated Ni-Nx sites on graphene defects.

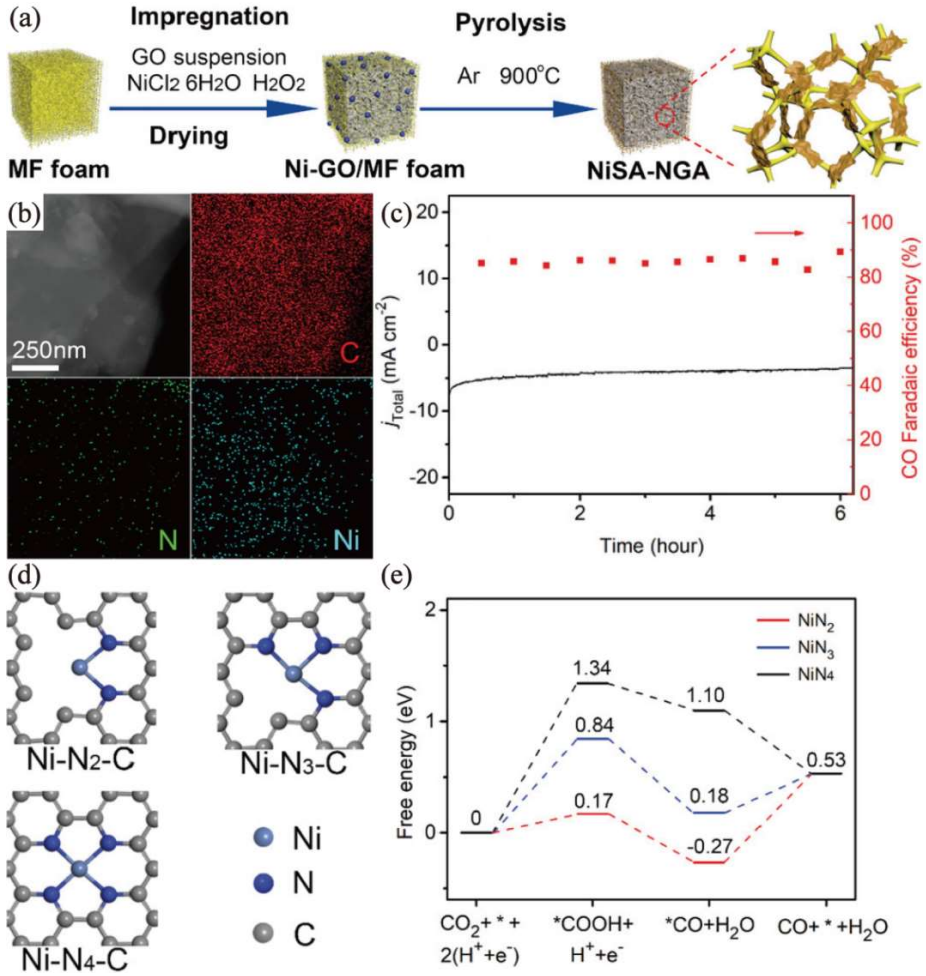

Figure 6. (a) Schematic illustration of the synthesis of NiSA-NGA; (b) STEM images and the corresponding EDS elemental maps of C, N, and Ni for NiSA-NGA; (c) Stability of total current density and the corresponding CO Faradaic efficiency of NiSA-NGA at electrolytic potentials of −0.8 V vs. RHE in 0.5 M $KHCO_3$ electrolyte; (d) Top view of Ni-N_2-C, Ni-N_3-C and Ni-N_4-C; (e) Free energy diagram for electrochemical reduction of CO_2 to CO on Ni-Nx sites (Ni-N_2, Ni-N_3 and Ni-N_4)[105].

Choi et al.[106] synthesized a 3D highly porous and conductive iron porphyrin/graphene hydrogel (FePGH) by hydrothermal treatment of cationic iron porphyrin (FeTMAP) and liquid crystalline graphene oxide (LCGO) (Figure 7a). FePGH exhibited flat and large graphene structures (Figure 7b).

ISSN: 2414-1895 DOI: 10.6919/ICJE.202406_10(6).0018

The positively charged FeTMAP helped to maintain the flat and large graphene oxide sheets through electrostatic interactions with the negatively charged carboxylate functionalities on the edge of LCGO as well as π-π interactions. FePGH exhibited higher strength and a more uniform deformation under compression (Figure 7c). Total geometrical current densities increased with the increasing amount of FeTMAP utilised for the formation of the FePGH (Figure 7d), which directly affected the catalytic activity for CO_2 reduction. Compared with FePGH-L (containing 0.6 mg FeTMAP), FePGH-H (containing 1.1 mg FeTMAP) obtained considerable current density with an enhanced CO conversion efficiency (Figure 7e). As a CO_2 reduction catalyst, FePGH benefits from various functional groups of 3D GH, which can integrate a number of catalytically active centres. In addition, hydrogels consist of highly porous structures. Formation of 3D porous conductive pathways along the graphene backbone facilitates gas diffusion and improves the catalytic conversion of CO_2. FePGH-H exhibited superior long-term durability at -0.39 V vs. RHE over 20 h electrolysis, affording a stable current density of 0.42 mA/cm^2 and 96.4% CO Faraday Efficiency (Figure 7f), showcasing excellent CO_2 reduction performance.

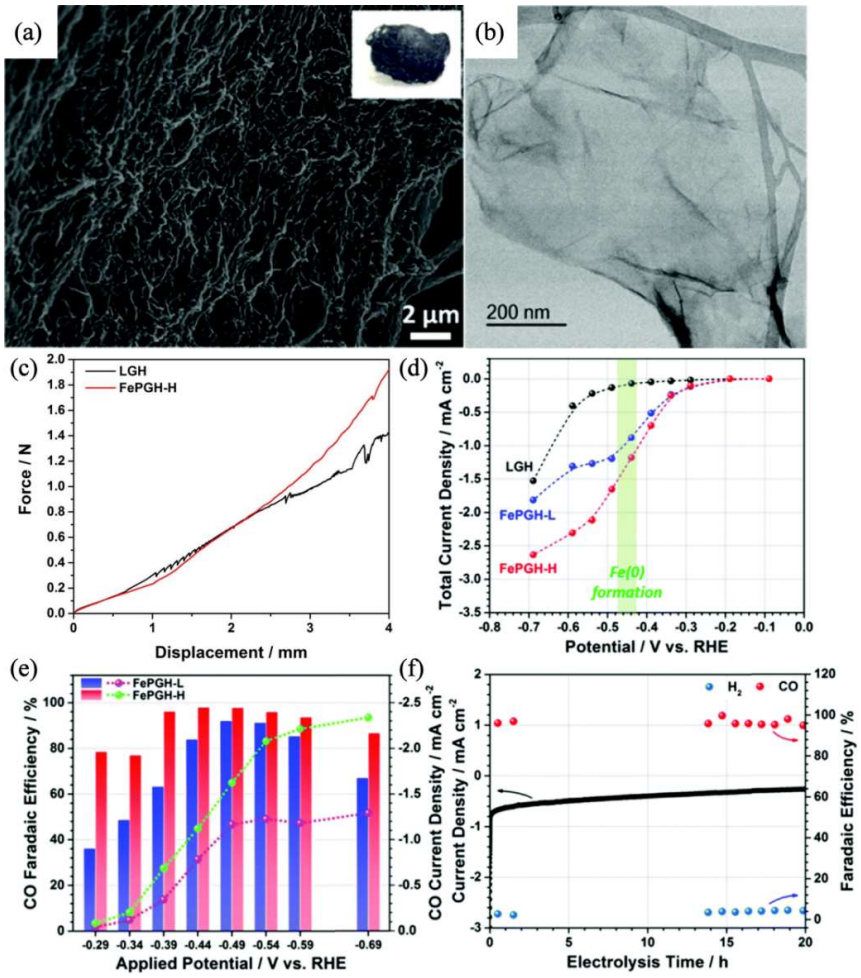

Figure 7. (a) SEM and (b) TEM images of FePGH; (c) Force versus displacement plots for LGH and FePGH; (d) Total current densities of LGH, FePGH-L and FePGH-H at different applied potentials with Fe(0) formation highlighted; (e) CO faradaic efficiencies (bar graph) and CO partial current densities (line graph) obtained by FePGH-L and FePGH-H; (f) Long-term stability at −0.39 V with respect to current density (black dots) and faradaic efficiency (coloured dots) of CO_2 reduction electrocatalysis by FePGH-H[106].

In the electrocatalytic system, combining the electrocatalyst with three-dimensional carbon gels can effectively enhance the electrocatalytic activity. On the one hand, the large specific surface area and

ISSN: 2414-1895 DOI: 10.6919/ICJE.202406_10(6).0018

pore volume allow the catalyst to be uniformly dispersed on the carbon carrier, exposing more active sites. The defects or functional groups on the surface can capture and anchor the catalyst, inhibiting the agglomeration of the catalyst and reducing the deactivation of the catalyst. On the other hand, 3D carbon gels have good mechanical properties and chemical stability. The high-strength porous structure helps the diffusion of CO_2 and product gases. In addition, its hydrophobicity suppresses the competitive HER and improves the CO_2 catalytic conversion performance.

3.3 Thermalcatalytic Reduction of CO_2

3.3.1 Principles of Thermocatalytic Reduction of CO_2

Utilizing CO_2 and H_2 for thermochemical conversion is one of the research hotspots in the fields of energy and environment. CO_2 thermocatalytic hydrogenation reactions are typically carried out at relatively low temperatures (≤523 K) for the production of high-value fuels and chemicals such as CH_4 and CH_3OH [107]. CO_2 molecules are thermodynamically and chemically stable and require a large amount of energy if used as single reactant. Introducing other substances with higher Gibbs free energy (e.g. H_2) as co-reactants can make the thermodynamic process more feasible [79].

In the thermocatalytic process, the reactant H_2 is more valuable than the products CH_4 and CH_3OH. Therefore, the hydrogen source for CO_2 thermocatalytic reduction is typically renewable H_2, derived from non-fossil sources. The H_2/CO_2 ratios for the hydrogenation of CO_2 to CH_4 and CH_3OH are 4 and 3, respectively, and a substantial amount of H_2 is required. From a thermodynamic perspective, converting CO_2 to CH_4 is the easier route [108]. Compared with the CH_3OH production process, CH_4 possesses a better energy storage capability [109].

$$CO_2 + 4H_2 \rightleftharpoons CH_4 + 2H_2O \quad \Delta H^{\circ}_{298} = -164.9 \text{ kJ/mol} \tag{1}$$

From Equation (1), it is evident that the methanation process is highly exothermic, while reactor overheating remains one of the technical difficulties to be fully solved. Moreover, high temperatures are not conducive to the exothermic and reversible methanation process [110,111], and also accelerate catalyst deactivation. Currently, significant challenges are faced in the development of thermocatalysts with high catalytic performance and long-term stability. These adverse conditions can be ameliorated by 3D carbon gels, which have a high specific surface area and porous structure and can be introduced into thermocatalysts as supports.

3.3.2 Application of Three-Dimensional Carbon Gels in Thermocatalytic CO_2 Reduction

Hu et al.[112] used ammonia as a cross-linking agent to mix $Ni(NO_3)_2 \cdot 6H_2O$ aqueous with GO, and prepared the thermocatalyst Ni/GA through a hydrothermal process. Ni/GA had a 3D network structure (Figure 8a). The high porosity and large specific surface area of GA provided more space for the loading of Ni species. GA exhibited strong interactions with Ni species, limiting the size of Ni particles. Ni species were evenly distributed in graphene sheets with small particle sizes, which effectively inhibited the aggregation of Ni (Figure 8b). The CH_4 yield of Ni/GA catalyst (76.2%) was higher than that of Ni/GO (63.9%) at 350 ℃ (Figure 8c). Compared with 2D GO, 3D GA facilitates better dispersion for Ni species, and the resulting smaller Ni particles can activate and dissociate hydrogen more effectively. The catalytic experiment for 80 h showed excellent stability of Ni/GA at both 300 and 450 ℃ (Figure 8d). The Ni/GA catalyst reached the highest CO_2 conversion (80.4%) and CH_4 selectivity (94.8%) at 350 ℃, both higher than the catalysts that Ni supported at GO and RGO. The transition from 2D to 3D structure contributes to the enhancement of catalytic performance.

Deerattrakul et al.[113] synthesized the reduced graphene oxide aerogel catalysts (CuZn/rGOae) loaded with Cu-Zn by hydrothermal method and incipient wetness impregnation, which were applied to thermocatalytic CO_2 hydrogenation to MeOH. The sample exhibited porous 3D framework structure (Figure 9a). Cu-Zn metal nanoparticles were uniformly dispersed on the graphene sheets (Figure 9b). The catalyst had the highest specific surface area (458 m^2/g) at the hydrothermal temperature of 140 ℃ (Figure 9c). The number of oxygen functionalities decreased with increasing

ISSN: 2414-1895 DOI: 10.6919/ICJE.202406_10(6).0018

hydrothermal reduction temperature (Figure 9d). Higher temperature led to restacking of graphene sheets and surface area drastically decreased. Low temperature lacked sufficient energy to form a high-porous 3D network of rGOae. The optimal loading rate of Cu-Zn metal was 15 wt%. Higher loading resulted in the greater agglomeration of metal nanoparticles, while lower loading led to the fewer catalytic active sites. The 15%Cu-Zn/rGOae-140℃ catalyst achieved the highest MeOH yield (94.53 $mg_{MeOH}/(g_{cat}\cdot h)$) at a reaction temperature of 250 ℃ and a pressure of 15 bar (Figure 9e).

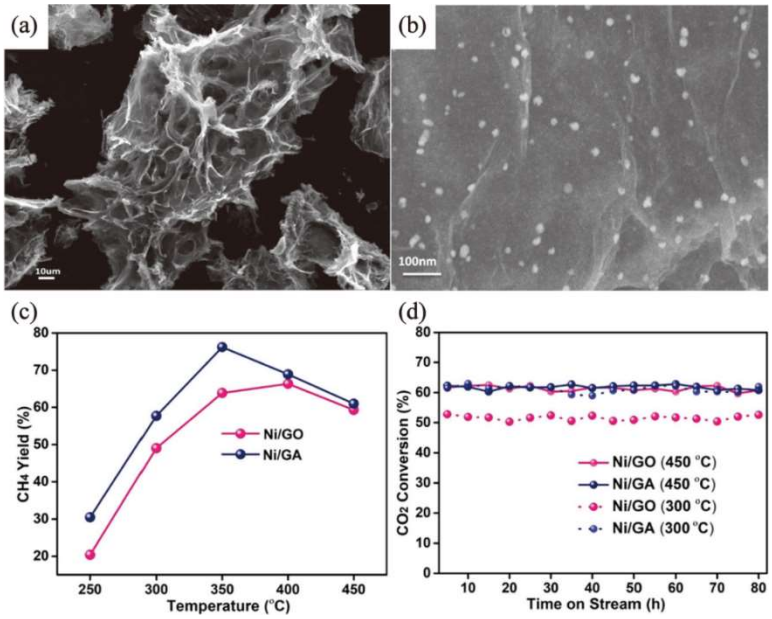

Figure 8. (a) and (b) SEM images of Ni/GA; (c) The yields of CH_4 for Ni/GO and Ni/GA at different temperatures; (d) The stability tests of the catalysts at 300 ℃ and 450 ℃[112].

The authors subsequently studied 15% CuZn/NrGOae [114], which is the nitrogen-doped reduced graphene oxide aerogel (NrGOae) loaded with 15 wt% Cu-Zn. The introduction of nitrogen impurities onto the graphene aerogel resulted in smaller size Cu-Zn particles that were uniformly dispersed on the graphene sheets of the porous aerogel (Figure 10a and b). The presence of N species (especially pyridine-N) facilitates the adsorption and activation of CO_2 as well as the dispersion of metals, which plays an important role in improving the catalytic performance. Different nitrogen sources resulted in varying nitrogen contents (Figure 10c). The catalyst, 15%CuZn/NrGOae-U (with urea as the nitrogen source), achieved the highest methanol space-time yield (405.49 $mg/(g_{cat}\cdot h)$) (Figure 10d). The highest spatiotemporal yield of MeOH (STY_{MeOH}) was 405.49 $mg/(g_{cat}\cdot h)$ for the 15% CuZn/NrGOae-U (nitrogen source was urea) catalyst (Fig. 10d). It can be seen that the 3D graphene aerogel with structural defects obtained by doping nitrogen promotes the CO_2 thermocatalytic hydrogenation reaction and improves the reduction yield.

In the thermocatalytic reduction of CO_2, the introduction of 3D carbon gel can improve the performance of the catalyst. On the one hand, the defects present in 3D carbon gels as well as the doped non-carbon elemental impurities can serve as active sites to improve CO_2 adsorption and catalytic reduction activity. On the other hand, prolonged high-temperature and high-pressure operation may cause structural fatigue of the catalyst, leading to structural collapse as well as damage to the active sites, thereby reducing the catalyst activity. 3D carbon gels have good thermal stability and high mechanical properties, which can be used as supports to extend the service life of the catalysts. In addition, agglomeration of the catalyst particles may occur at high temperatures. The porous structure of the carbon gel has a large surface area, which can uniformly disperse and anchor the catalyst, inhibiting its agglomeration and deactivation.

ISSN: 2414-1895 DOI: 10.6919/ICJE.202406_10(6).0018

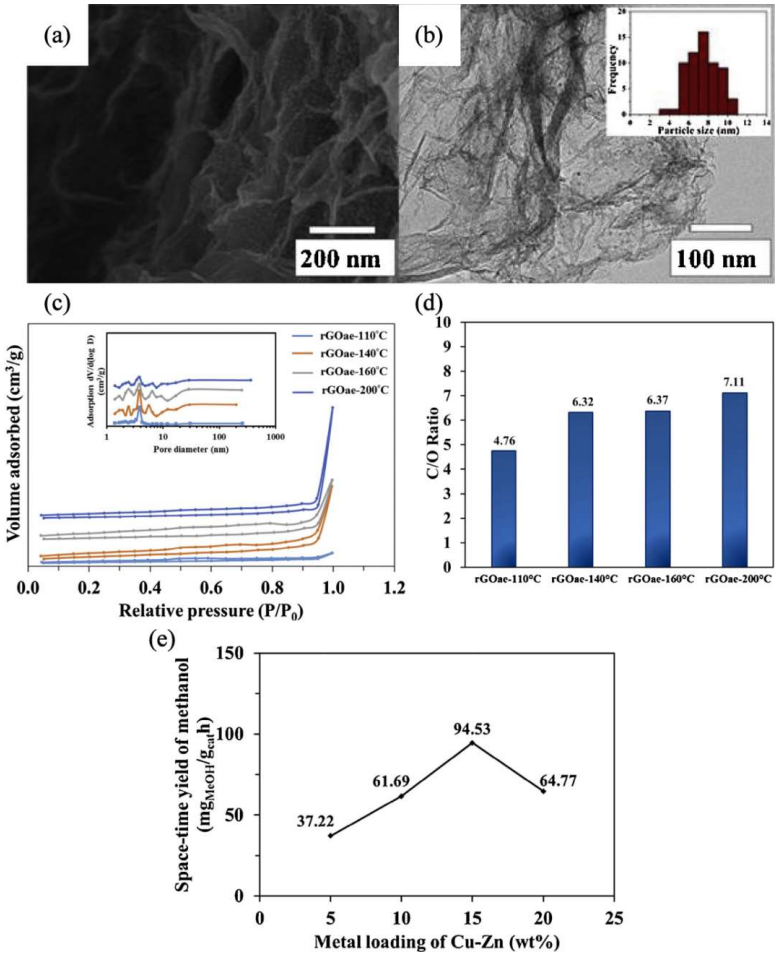

Figure 9. (a) FE-SEM and (b) TEM images of CuZn/rGOae–140 ℃ with the amounts of 15% Cu-Zn; (c) N_2 adsorption-desorption isotherms of rGOae-T (T=110 ℃, 140 ℃, 160 ℃ and 200 ℃); (d) C/O atomic ratios of rGOae at different reduction temperatures; (e) Space-time yield of methanol at 250 ℃, 15 bar, GHSV of 2 444.397 9 h^{-1}[113].

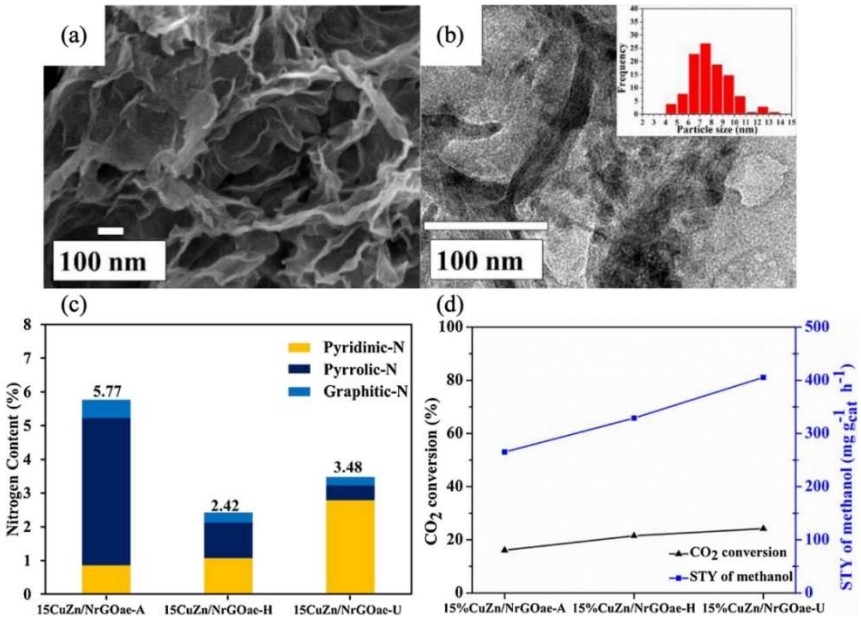

Figure 10. (a) FE-SEM and (b)TEM images of 15%CuZn/NrGOae-U; (c) specific nitrogen contents of the as-prepared catalysts; (d) CO_2 conversion and space-time yield of methanol at 250 ℃ and 15 bar of CO_2[114].

ISSN: 2414-1895 DOI: 10.6919/ICJE.202406_10(6).0018

4. Summary and Outlook

Catalytic Reduction of CO_2 holds promising prospects as a research frontier, aiming to utilize electrical and thermal energy generated from solar power or other renewable sources for the conversion of CO_2 into high-value products, thereby achieving carbon neutrality. This paper provides an overview of the research progress on the utilization of three-dimensional carbon gels for catalytic CO_2 reduction, addressing common challenges encountered in photocatalytic, electrocatalytic, and thermocatalytic CO_2 reduction.

Three-dimensional carbon gels exhibit a substantial specific surface area, high porosity, and excellent electrical conductivity, characteristics that can enhance the rate and efficiency of catalytic reactions. In comparison to one-dimensional and 2D carbon materials, the superior network structure of 3D carbon gels not only facilitates better dispersion and prevents aggregation of loaded catalysts but also provides multidimensional pathways for mass and electron transfer during catalytic reactions. Additionally, three-dimensional carbon gels possess robust thermal stability, chemical durability, and high mechanical strength, indicating that catalysts supported on 3D carbon gels exhibit a degree of resistance to adverse environmental conditions. Notably, the high CO_2 adsorption capacity of three-dimensional carbon aerogels constitutes a crucial attribute, establishing a solid foundation for their application as catalyst supports in CO_2-related processes.

Despite substantial advancements, challenges and issues associated with 3D carbon gels remain to be addressed. Firstly, the synthesis of 3D carbon gels with precise dimensions, structures, and spatial arrangements significantly influences the size and catalytic performance of loaded catalysts. Secondly, while enriched CO_2 is typically employed in catalytic CO_2 reduction experiments, achieving high selectivity adsorption of CO_2 in the presence of competing gases is crucial for practical applications. This might require comprehensive adjustments in pore structure, carbon gel modification, and microenvironmental factors such as hydrophobic/hydrophilic properties and active sites. Additionally, gaining a deeper understanding of the interactions between reactants/intermediates/products and 3D carbon gel catalysts is essential for enhancing catalytic efficiency and developing the next generation of such catalysts. CO_2 reduction pathways involve multiple proton and electron transfer processes, encompassing various products and related reaction intermediates. For complex CO_2 reduction processes, establishing suitable theoretical models for catalytic mechanisms will necessitate the integration of advanced characterization techniques and precise theoretical calculations. Finally, efforts to improve the stability, product selectivity, and reaction activity of 3D carbon gel-based catalysts in CO_2 catalysis are still required.

Currently, the combination of photocatalytic, electrocatalytic, and thermal catalytic systems to create synergistic setups that enhance CO_2 catalytic conversion efficiency is emerging as a novel direction in CO_2 catalysis research. As research deepens, it is anticipated that the catalytic performance of 3D carbon gel-based catalysts will further improve, propelling the development of the CO_2 catalysis field.

References

[1] Okoye-Chine, C.G.; Otun, K.; Shiba, N.; Rashama, C.; Ugwu, S.N.; Onyeaka, H.; Okeke, C.T. Conversion of carbon dioxide into fuels—a review. Journal of CO2 Utilization. 2022, 62, 102099.

[2] Jeffry, L.; Ong, M.Y.; Nomanbhay, S.; Mofijur, M.; Mubashir, M.; Show, P.L. Greenhouse gases utilization: A review. Fuel. 2021, 301, 121017.

[3] Park, J.H.; Yang, J.; Kim, D.; Gim, H.; Choi, W.Y.; Lee, J.W. Review of recent technologies for transforming carbon dioxide to carbon materials. Chemical Engineering Journal. 2022, 427, 130980.

[4] Shehzad, N.; Tahir, M.; Johari, K.; Murugesan, T.; Hussain, M. A critical review on TiO2 based photocatalytic CO2 reduction system: Strategies to improve efficiency. Journal of CO2 Utilization. 2018, 26, 98-122.

[5] Francke, R.; Schille, B.; Roemelt, M. Homogeneously catalyzed electroreduction of carbon dioxide-methods, mechanisms, and catalysts. Chemical reviews. 2018, 118, 4631-4701.

ISSN: 2414-1895 DOI: 10.6919/ICJE.202406_10(6).0018

[6] Hasani, A.; Tekalgne, M.; Van Le, Q.; Jang, H.W.; Kim, S.Y. Two-dimensional materials as catalysts for solar fuels: hydrogen evolution reaction and CO2 reduction. Journal of Materials Chemistry A. 2019, 7, 430-454.

[7] Wang, L.; Chen, W.; Zhang, D.; Du, Y.; Amal, R.; Qiao, S.; Wu, J.; Yin, Z. Surface strategies for catalytic CO2 reduction: from two-dimensional materials to nanoclusters to single atoms. Chemical Society Reviews. 2019, 48, 5310-5349.

[8] Zhang, Z.; Zheng, Y.; Qian, L.; Luo, D.; Dou, H.; Wen, G.; Yu A.; Chen, Z. Emerging Trends in Sustainable CO2-Management Materials. Advanced Materials. 2022, 34, 2201547.

[9] Liu, M.; Nothling, M.D.; Zhang, S.; Fu, Q.; Qiao, G.G. Thin film composite membranes for postcombustion carbon capture: Polymers and beyond. Progress in Polymer Science. 2022, 126, 101504.

[10] Wang, W.H.; Himeda, Y.; Muckerman, J.T.; Manbeck, G.F.; Fujita, E. CO2 hydrogenation to formate and methanol as an alternative to photo- and electrochemical CO2 reduction. Chemical reviews. 2015, 115, 12936-12973.

[11] Notz, D.; Stroeve, J. Observed Arctic sea-ice loss directly follows anthropogenic CO2 emission. Science. 2016, 354, 747-750.

[12] Verma, S.; Lu, S.; Kenis, P.J. Co-electrolysis of CO2 and glycerol as a pathway to carbon chemicals with improved technoeconomics due to low electricity consumption. Nature Energy. 2019, 4, 466-474.

[13] Li, X.; Yu, J.; Jaroniec, M.; Chen, X. Cocatalysts for selective photoreduction of CO2 into solar fuels. Chemical reviews. 2019, 119, 3962-4179.

[14] Kapsenberg, L.; Cyronak, T. Ocean acidification refugia in variable environments. Global Change Biology. 2019, 25, 3201-3214.

[15] Doney, S.C.; Busch, D.S.; Cooley, S.R.; Kroeker, K.J. The Impacts of Ocean Acidification on Marine Ecosystems and Reliant Human Communities. Annual Review of Environment and Resources. 2020, 45, 83-112.

[16] Doo, S.S.; Kealoha, A.; Andersson, A.; Cohen, A.L.; Hicks, T.L.; Johnson, Z.I.; Long, M.H.; McElhany, P.; Mollica, N.; Shamberger, K.E.F.; Silbiger, N.J.; Takeshita, Y.; Busch, D.S. The challenges of detecting and attributing ocean acidification impacts on marine ecosystems. ICES Journal of Marine Science. 2020, 77, 2411-2422.

[17] Piñango, A.; Kerr, R.; Orselli, I.B.M.; Carvalho, A.D.C.O.; Azar, E.; Karstensen, J.; Garcia, C.A.E. Ocean Acidification and Long-Term Changes in the Carbonate System Properties of the South Atlantic Ocean. Global Biogeochemical Cycles. 2022, 36, e2021GB007196.

[18] Albright, R.; Hansson, L.; Cooley, S.R.; Gattuso, J.P.; Marshall, P.; Marshall, N.; Fletcher, S.; Haraldsson, G.; Hoegh-Guldberg, O. Are we ready for ocean acidification? A framework for assessing and advancing policy readiness. Environmental Research Letters. 2023, 18, 041001.

[19] Jiang, L.Q.; Dunne, J.; Carter, B.R.; Tjiputra, J.F.; Terhaar, J.; Sharp, J.D.; Olsen, A.; Alin, S.; Bakker, D.C.E.; Feely, R.A.; Gattuso, J.P.; Hogan, P.; Ilyina, T.; Lange, N.; Lauvset, S.K.; Lewis, E.R.; Lovato, T.; Palmieri, J.; Santana-Falcón, Y.; Schwinger, J.; Séférian, R.; Strand, G.; Swart, N.; Tanhua, T.; Tsujino, H.; Wanninkhof, R.; Watanabe, M.; Yamamoto, A.; Ziehn, T. Global Surface Ocean Acidification Indicators From 1750 to 2100. Journal of Advances in Modeling Earth Systems. 2023, 15, e2022MS003563.

[20] Manríquez, P.H.; Gonzalez, C.P.; Seguel, M.; Garcia-Huidobro, M.R.; Lohrmann, K.B.; Domenici, P.; Watson, S.; Duarte, C.; Brokordt, K. The combined effects of ocean acidification and warming on a habitat-forming shell-crushing predatory crab. Science of the Total Environment. 2021, 758, 143587.

[21] Thangal, S.H.; Muralisankar, T.; Anandhan, K.; Gayathri, V.; Yogeshwaran, A. Effect of CO2 driven ocean acidification on the mud crab Scylla serrata instars. Environmental Pollution. 2022, 312, 119995.

[22] Cui, D.; Liu, L.; Zhao, T.; Zhan, Y.; Song, J.; Zhang, W.; Yin, D.; Chang, Y. Responses of sea urchins (Strongylocentrotus intermedius) with different sexes to CO2-induced seawater acidification: Histology, physiology, and metabolomics. Marine Pollution Bulletin. 2022, 178, 113606.

[23] Xu, M.; Sun, T.; Tang, X.; Lu, K.; Jiang, Y.; Cao, S.; Wang, Y. CO2 and HCl-induced seawater acidification impair the ingestion and digestion of blue mussel Mytilus edulis. Chemosphere. 2020, 240, 124821.

ISSN: 2414-1895 DOI: 10.6919/ICJE.202406_10(6).0018

[24] Wilson-McNeal, A.; Hird, C.; Hobbs, C.; Nielson, C.; Smith, K.E.; Wilson, R.W.; Lewis, C. Fluctuating seawater pCO2/pH induces opposing interactions with copper toxicity for two intertidal invertebrates. Science of the Total Environment. 2020, 748, 141370.

[25] Yu, X.; Liu, J.; Qiu, T.; Cao, L.; Dou, S. Ocean acidification induces tissue-specific interactions with copper toxicity on antioxidant defences in viscera and gills of Asiatic hard clam Meretrix petechialis (Lamarck, 1818). Science of The Total Environment. 2023, 875, 162634.

[26] Xiao, Z.; Cao, L.; Liu, J.; Cui, W.; Dou, S. pCO2-driven seawater acidification affects aqueous-phase copper toxicity in juvenile flounder Paralichthys olivaceus: Metal accumulation, antioxidant defenses and detoxification in livers. Science of The Total Environment. 2023, 858, 160040.

[27] Sartori, D.; Scatena, G.; Vrinceanu, C.A.; Gaion, A. Increased sensitivity of sea urchin larvae to metal toxicity as a consequence of the past two decades of Climate Change and Ocean Acidification in the Mediterranean Sea. Marine Pollution Bulletin. 2023, 194, 115274.

[28] Xie, J.; Sun, X.; Li, P.; Zhou, T.; Jiang, R.; Wang, X. The impact of ocean acidification on the eye, cuttlebone and behaviors of juvenile cuttlefish (Sepiella inermis). Marine Pollution Bulletin. 2023, 190, 114831.

[29] Gür, T.M. Carbon dioxide emissions, capture, storage and utilization: Review of materials, processes and technologies. Progress in Energy and Combustion Science. 2022, 89, 100965.

[30] Osman, A.I.; Hefny, M.; Abdel Maksoud, M.I.A.; Elgarahy, A.M.; Rooney, D.W. Recent advances in carbon capture storage and utilisation technologies: a review. Environmental Chemistry Letters. 2021, 19, 797-849.

[31] Nocito, F.; Dibenedetto, A. Atmospheric CO2 mitigation technologies: carbon capture utilization and storage. Current Opinion in Green and Sustainable Chemistry. 2020, 21, 34-43.

[32] Yang, Y.; Xu, W.; Wang, Y.; Shen, J.; Wang, Y.; Geng, Z.; Wang, Q.; Zhu, T. Progress of CCUS technology in the iron and steel industry and the suggestion of the integrated application schemes for China. Chemical Engineering Journal. 2022, 450, 138438.

[33] Zhao, K.; Jia, C.; Li, Z.; Du, X.; Wang, Y.; Li, J.; Yao, Z.; Yao, J. Recent Advances and Future Perspectives in Carbon Capture, Transportation, Utilization, and Storage (CCTUS) Technologies: A Comprehensive Review. Fuel. 2023, 351, 128913.

[34] Dziejarski, B.; Krzyżyńska, R.; Andersson, K. Current status of carbon capture, utilization, and storage technologies in the global economy: A survey of technical assessment. Fuel. 2023, 342, 127776.

[35] Chen, S.; Liu, J.; Zhang, Q.; Teng, F.; McLellan, B.C. A critical review on deployment planning and risk analysis of carbon capture, utilization, and storage (CCUS) toward carbon neutrality. Renewable and Sustainable Energy Reviews. 2022, 167, 112537.

[36] Yu, J.; Xie, L.H.; Li, J.R.; Ma, Y.; Seminario, J.M.; Balbuena, P.B. CO2 capture and separations using MOFs: computational and experimental studies. Chemical reviews. 2017, 117, 9674-9754.

[37] Vitillo, J.G.; Smit, B.; Gagliardi, L. Introduction: carbon capture and separation. Chemical Reviews. 2017, 117, 9521-9523.

[38] Keith, D.W.; Holmes, G.; Angelo, D.S.; Heidel, K. A process for capturing CO2 from the atmosphere. Joule. 2018, 2, 1573-1594.

[39] Zhang, Y.; Yu, L.; Cui, K.; Wang, H.; Fu, T. Carbon capture and storage technology by steel-making slags: Recent progress and future challenges. Chemical Engineering Journal. 2023, 455, 140552.

[40] Yu, X.; Catanescu, C.O.; Bird, R.E.; Satagopan, S.; Baum, Z.J.; Lotti Diaz, L.M.; Zhou, Q.A. Trends in Research and Development for CO2 Capture and Sequestration. ACS Omega. 2023, 8, 11643-11664.

[41] Wilberforce, T.; Baroutaji, A.; Soudan, B.; Al-Alami, A.H.; Olabi, A.G. Outlook of carbon capture technology and challenges. Science of the total environment, 2019, 657, 56-72.

[42] Elmobarak, W.F.; Almomani, F.; Tawalbeh, M.; Al-Othman, A.; Martis, R.; Rasool, K. Current status of CO2 capture with ionic liquids: Development and progress. Fuel. 2023, 344, 128102.

[43] Jiang, L.; Liu, W.; Wang, R.Q.; Gonzalez-Diaz, A.; Rojas-Michaga, M.F.; Michailos, S.; Pourkashanian, M.; Zhang, X.J.; Font-Palma, C. Sorption direct air capture with CO2 utilization. Progress in Energy and Combustion Science. 2023, 95, 101069.

ISSN: 2414-1895 DOI: 10.6919/ICJE.202406_10(6).0018

[44] Galán, G.; Martín, M.; Grossmann, I.E. Systematic comparison of natural and engineering methods of capturing CO2 from the air and its utilization. Sustainable Production and Consumption. 2023, 37, 78-95.

[45] Wang, J.; Fu, R.; Wen, S.; Ning, P.; Helal, M.H.; Salem, M.A.;Xu, B.B.; El-Bahy, Z.M.; Huang, M.; Guo, Z.; Huang, L.; Wang, Q. Progress and current challenges for CO2 capture materials from ambient air. Advanced Composites and Hybrid Materials. 2022, 5, 2721-2759.

[46] Ma, Z.; Ranjith, P.G. Review of application of molecular dynamics simulations in geological sequestration of carbon dioxide. Fuel. 2019, 255, 115644.

[47] Li, L.; Zhang, X.; Liu, J.; Xie, Q.; Zhou, X.; Zheng, J.; Su, Y. Research Progress and Prospect of Carbon Dioxide Utilization and Storage Based on Unconventional Oil and Gas Development. Energies. 2022, 15, 9383.

[48] Li, N.; Feng, W.; Yu, J.; Chen, F.; Zhang, Q.; Zhu, S.; Hu, Y.; Li, Y. Recent Advances in Geological Storage: Trapping Mechanisms, Storage Sites, Projects, and Application of Machine Learning. Energy & Fuels. 2023, 37, 10087-10111.

[49] Zhang, C.; Wang, M. CO2/brine interfacial tension for geological CO2 storage: A systematic review. Journal of Petroleum Science and Engineering. 2023, 220, 111154.

[50] Wu, S.; Wang, H.; Yuan, G.; Hu, B.; Sun, Z.; Yan, S.; Li, Y. Carbon Dioxide Flow Behavior through Nanopores: Implication for CO2 Sequestration in Unconventional Gas Reservoirs. Industrial & Engineering Chemistry Research. 2022, 61, 16869-16882.

[51] Rathnaweera, T.D.; Ranjith, P.G. Nano-modified CO2 for enhanced deep saline CO2 sequestration: A review and perspective study. Earth-Science Reviews. 2020, 200, 103035.

[52] Shen, Z.; Meng, Z. Enhancing the Efficiency of Coal Bed Methane Recovery by Injecting Carbon Dioxide Based on an Anthracite Coal Macromolecular Model and Simulation Methods. Energy & Fuels. 2022, 36, 6329-6342.

[53] Teng, Y.; Zhang, D. Long-term viability of carbon sequestration in deep-sea sediments. Science advances. 2018, 4, eaao6588.

[54] Kumar, Y.; Sangwai, J.S. A Perspective on the Effect of Physicochemical Parameters, Macroscopic Environment, Additives, and Economics to Harness the Large-Scale Hydrate-Based CO2 Sequestration Potential in Oceans. ACS Sustainable Chemistry & Engineering. 2023, 11, 10950-10979.

[55] Ning, Y.; Wang, L.; Yu, X.; Li, J. Recent development in the decarbonization of marine and offshore engineering systems. Ocean Engineering. 2023, 280, 114883.

[56] Qureshi, M.F.; Zheng, J.; Khandelwal, H.; Venkataraman, P.; Usadi, A.; Barckholtz, T.A.; Mhadeshwar, A.B.; Linga, P. Laboratory demonstration of the stability of CO2 hydrates in deep-oceanic sediments. Chemical Engineering Journal. 2022, 432, 134290.

[57] Xiao, T.; Wang, B.; Xu, L.; Esser, R.; Dai, Z.; Cather, M.; McPherson, B. Underground sources of drinking water chemistry changes in response to potential CO2 leakage. Science of The Total Environment. 2022, 847, 157254.

[58] Lee, S.Y.; Lee, J.U.; Lee, I.B.; Han, J. Design under uncertainty of carbon capture and storage infrastructure considering cost, environmental impact, and preference on risk. Applied Energy. 2017, 189, 725-738.

[59] Kim, C.; Yoo, C.J.; Oh, H.S.; Min, B.K.; Lee, U. Review of carbon dioxide utilization technologies and their potential for industrial application. Journal of CO2 Utilization. 2022, 65, 102239.

[60] Tang, B.; Xiao, F.X. An overview of solar-driven photoelectrochemical CO2 conversion to chemical fuels. ACS Catalysis. 2022, 12, 9023-9057.

[61] Liu, S.; Wang, M.; Cheng, Q.; He, Y.; Ni, J.; Liu, J.; Yan, C.; Qian, T. Turning waste into wealth: sustainable production of high-value-added chemicals from catalytic coupling of carbon dioxide and nitrogenous small molecules. ACS nano. 2022, 16, 17911-17930.

[62] Fu, L.; Ren, Z.; Si, W.; Ma, Q.; Huang, W.; Liao, K.; Huang, Z.; Wang, Y.; Li, J.; Xu, P. Research progress on CO2 capture and utilization technology. Journal of CO2 Utilization. 2022, 66, 102260.

[63] Zhang, Z.; Yi, P.; Hu, S.; Jin, Y. Achieving artificial carbon cycle via integrated system of high-emitting industries and CCU technology: Case of China. Journal of Environmental Management. 2023, 340, 118010.

ISSN: 2414-1895 DOI: 10.6919/ICJE.202406_10(6).0018

[64] Zhang, L.; Song, Y.; Shi, J.; Shen, Q.; Hu, D.; Gao, Q.; Chen, W.; Kow, K.W.; Pang, C.; Sun, N.; Wei, W. Frontiers of CO2 Capture and Utilization (CCU) towards Carbon Neutrality. Advances in Atmospheric Sciences. 2022, 39, 1252-1270.

[65] Sekizawa, K.; Sato, S.; Arai, T.; Morikawa, T. Solar-driven photocatalytic CO2 reduction in water utilizing a ruthenium complex catalyst on p-type Fe2O3 with a multiheterojunction. ACS Catalysis. 2018, 8, 1405-1416.

[66] Ran, J.; Jaroniec, M.; Qiao, S.Z. Cocatalysts in semiconductor-based photocatalytic CO2 reduction: achievements, challenges, and opportunities. Advanced materials. 2018, 30, 1704649.

[67] Lian, S.; Kodaimati, M.S.; Weiss, E.A. Photocatalytically active superstructures of quantum dots and iron porphyrins for reduction of CO2 to CO in water. ACS nano. 2018, 12, 568-575.

[68] Wu, H.L.; Li, X.B.; Tung, C.H.; Wu, L.Z. Semiconductor quantum dots: an emerging candidate for CO2 photoreduction. Advanced Materials. 2019, 31, 1900709.

[69] Wang, C.; Sun, Z.; Zheng, Y.; Hu, Y.H. Recent progress in visible light photocatalytic conversion of carbon dioxide. Journal of Materials Chemistry A. 2019, 7, 865-887.

[70] Wang, J.; Ji, Y.; Shao, Q.; Yin, R.; Guo, J.; Li, Y.; Huang, X. Phase and structure modulating of bimetallic CuSn nanowires boosts electrocatalytic conversion of CO2. Nano Energy. 2019, 59, 138-145.

[71] Nitopi, S.; Bertheussen, E.; Scott, S.B.; Liu, X.; Engstfeld, A.K.; Horch, S.; Seger, B.; Stephens, I.E.L.; Chan, K.; Hahn, C.; Nørskov, J.K.; Jaramillo, T.F.; Chorkendorff, I. Progress and perspectives of electrochemical CO2 reduction on copper in aqueous electrolyte. Chemical reviews. 2019, 119, 7610-7672.

[72] Wang, W.; Shang, L.; Chang, G.; Yan, C.; Shi, R.; Zhao, Y.; Waterhouse, G.I.N.; Yang, D.; Zhang, T. Intrinsic carbon-defect-driven electrocatalytic reduction of carbon dioxide. Advanced Materials. 2019, 31, 1808276.

[73] Fan, Q.; Hou, P.; Choi, C.; Wu, T.S.; Hong, S.; Li, F.; Soo, Y.; Sun, Z. Activation of Ni particles into single Ni–N atoms for efficient electrochemical reduction of CO2. Advanced Energy Materials. 2020, 10, 1903068.

[74] Albero, J.; Peng, Y.; García, H. Photocatalytic CO2 Reduction to C2+ Products. ACS Catalysis. 2020, 10, 5734.

[75] Fan, L.; Xia, C.; Yang, F.; Wang, J.; Wang, H.; Lu, Y. Strategies in catalysts and electrolyzer design for electrochemical CO2 reduction toward C2+ products. Science advances. 2020, 6, eaay3111.

[76] Fan, L.; Xia, C.; Zhu, P.; Lu, Y.; Wang, H. Electrochemical CO2 reduction to high-concentration pure formic acid solutions in an all-solid-state reactor. Nature communications. 2020, 11, 3633.

[77] Zhang, J.C.; Ge, B.H.; Liu, T.F.; Yang, Y.Z.; Li, B.; Li, W.Z. Robust ruthenium-saving catalyst for high-temperature carbon dioxide reforming of methane. Acs Catalysis. 2019, 10, 783-791.

[78] Baddour, F.G.; Roberts, E.J.; To, A.T.; Wang, L.; Habas, S.E.; Ruddy, D.A.;Bedford, N.M.; Wright, J.; Nash, C.P.; Schaidle, J.A.; Brutchey, R.L.; Malmstadt, N. An exceptionally mild and scalable solution-phase synthesis of molybdenum carbide nanoparticles for thermocatalytic CO2 hydrogenation. Journal of the American Chemical Society. 2020, 142, 1010-1019.

[79] Jiang, X.; Nie, X.; Guo, X.; Song, C.; Chen, J.G. Recent advances in carbon dioxide hydrogenation to methanol via heterogeneous catalysis. Chemical reviews. 2020, 120, 7984-8034.

[80] Zhang, W.; Mohamed, A.R.; Ong, W.J. Z-Scheme photocatalytic systems for carbon dioxide reduction: where are we now?. Angewandte Chemie International Edition. 2020, 59, 22894-22915.

[81] Chang, X.; Wang, T.; Yang, P.; Zhang, G.; Gong, J. The development of cocatalysts for photoelectrochemical CO2 reduction. Advanced Materials. 2019, 31, 1804710.

[82] Zhang, N.; Long, R.; Gao, C.; Xiong, Y. Recent progress on advanced design for photoelectrochemical reduction of CO2 to fuels. Science China Materials. 2018, 61, 771-805.

[83] Fu, J.; Jiang, K.; Qiu, X.; Yu, J.; Liu, M. Product selectivity of photocatalytic CO2 reduction reactions. Materials Today. 2020, 32, 222-243.

[84] Zhou, Y.; Wang, Z.; Huang, L.; Zaman, S.; Lei, K.; Yue, T.; Li, Z.; You, B.; Xia, B.Y. Engineering 2D photocatalysts toward carbon dioxide reduction. Advanced Energy Materials. 2021, 11, 2003159.

ISSN: 2414-1895 DOI: 10.6919/ICJE.202406_10(6).0018

[85] Khan, A.A.; Tahir, M. Recent advancements in engineering approach towards design of photo-reactors for selective photocatalytic CO2 reduction to renewable fuels. Journal of CO2 Utilization. 2019, 29, 205-239.

[86] Vu, N.N.; Kaliaguine, S.; Do, T.O. Critical aspects and recent advances in structural engineering of photocatalysts for sunlight-driven photocatalytic reduction of CO2 into fuels. Advanced Functional Materials. 2019, 29, 1901825.

[87] Kovacic, Z.; Likozar, B.; Hus, M. Photocatalytic CO2 reduction: A review of ab initio mechanism, kinetics, and multiscale modeling simulations. ACS catalysis. 2020, 10, 14984-15007.

[88] Qiu, L.Q.; Yao, X.; Zhang, Y.K.; Li, H.R.; He, L.N. Advancements and challenges in reductive conversion of carbon dioxide via thermo-/photocatalysis. The Journal of Organic Chemistry. 2022, 88, 4942-4964.

[89] Zhang, L.; Zhao, Z.J.; Gong, J. Nanostructured materials for heterogeneous electrocatalytic CO2 reduction and their related reaction mechanisms. Angewandte Chemie International Edition. 2017, 56, 11326-11353.

[90] Han, N.; Ding, P.; He, L.; Li, Y.; Li, Y. Promises of main group metal–based nanostructured materials for electrochemical CO2 reduction to formate. Advanced Energy Materials. 2020, 10, 1902338.

[91] Sun, H.; Xu, Z.; Gao, C. Multifunctional, ultra-flyweight, synergistically assembled carbon aerogels. Advanced materials. 2013, 25, 2554-2560.

[92] Hwang, M.; Kang, J.; Seong, K.D.; Kim, D.K.; Jin, X.; Antink, W.H.; Lee, C.; Piao, Y. Ni-Co hydroxide nanoneedles embedded in graphene hydrogel as a binder-free electrode for high-performance asymmetric supercapacitor. Electrochimica Acta. 2018, 270, 156-164.

[93] Zhu, J.; Yang, X.; Fu, Z.; Wang, C.; Wu, W.; Zhang, L. Facile fabrication of ultra-low density, high-surface-area, broadband antireflective carbon aerogels as ultra-black materials. Journal of Porous Materials. 2016, 23, 1217-1225.

[94] Xiao, M.; Wang, Z.; Lyu, M.; Luo, B.; Wang, S.; Liu, G.; Cheng, H.; Wang, L. Hollow nanostructures for photocatalysis: advantages and challenges. Advanced Materials. 2019, 31, 1801369.

[95] Ali, S.; Humayun, M.; Pi, W.; Yuan, Y.; Wang, M.; Khan, A.; Yue, P.; Shu, L.; Zheng, Z.; Fu, Q.; Luo, W. Fabrication of BiFeO3-g-C3N4-WO3 Z-scheme heterojunction as highly efficient visible-light photocatalyst for water reduction and 2,4-dichlorophenol degradation: insight mechanism. Journal of hazardous materials. 2020, 397, 122708.

[96] Huang, G.; Curt, S.R.; Wang, K.; Markides, C.N. Challenges and opportunities for nanomaterials in spectral splitting for high-performance hybrid solar photovoltaic-thermal applications: a review. Nano Materials Science. 2020, 2, 183-203.

[97] Jung, H.; Cho, K.M.; Kim, K.H.; Yoo, H.W.; Al-Saggaf, A.; Gereige, I.; Jung, H.T. Highly efficient and stable CO2 reduction photocatalyst with a hierarchical structure of mesoporous TiO2 on 3D graphene with few-layered MoS2. ACS Sustainable Chemistry & Engineering. 2018, 6, 5718-5724.

[98] Yang, M.; Wang, P.; Li, Y.; Tang, S.; Lin, X.; Zhang, H.; Zhu, Z.; Chen, F. Graphene aerogel-based NiAl-LDH/g-C3N4 with ultratight sheet-sheet heterojunction for excellent visible-light photocatalytic activity of CO2 reduction. Applied Catalysis B: Environmental. 2022, 306, 121065.

[99] Zhao, X.; Xu, M.; Song, X.; Zhou, W.; Liu, X.; Wang, H.; Huo, P. Integration of 3D macroscopic reduced graphene oxide aerogel with DUT-67 for selective CO2 photoreduction to CO in Gas-Solid reaction. Chemical Engineering Journal. 2022, 446, 137034.

[100] Huang, J.; Chen, Y. Combining theory and experiment in advancing fundamental electrocatalysis. Current Opinion in Electrochemistry. 2019, 14, A4-A9.

[101] Chen, Y.; Zhang, J.; Yang, L.; Wang, X.; Wu, Q.; Hu, Z. Recent advances in non-precious metal–nitrogen–carbon single-site catalysts for CO2 electroreduction reaction to CO. Electrochemical Energy Reviews. 2022, 5, 11.

[102] Bard, A.J. Inner-sphere heterogeneous electrode reactions. Electrocatalysis and photocatalysis: the challenge. Journal of the American Chemical Society. 2010, 132, 7559-7567.

[103] Dunwell, M.; Yan, Y.; Xu, B. Understanding the influence of the electrochemical double-layer on heterogeneous electrochemical reactions. Current opinion in chemical engineering. 2018, 20, 151-158.

[104] Xiao, X.; Xu, Y.; Lv, X.; Xie, J.; Liu, J.; Yu, C. Electrochemical CO2 reduction on copper nanoparticles-dispersed carbon aerogels. Journal of colloid and interface science. 2019, 545, 1-7.

ISSN: 2414-1895 DOI: 10.6919/ICJE.202406_10(6).0018

[105] Mou, K.; Chen, Z.; Zhang, X.; Jiao, M.; Zhang, X.; Ge, X.; Zhang, W.; Liu, L. Highly efficient electroreduction of CO2 on nickel single-atom catalysts: atom trapping and nitrogen anchoring. Small. 2019, 15, 1903668.

[106] Choi, J.; Kim, J.; Wagner, P.; Gambhir, S.; Jalili, R.; Byun, S.; Sayyar, S.; Lee, Y.M.; MacFarlane, D.R.; Wallace, G.G.; Officer, D.L. Energy efficient electrochemical reduction of CO2 to CO using a three-dimensional porphyrin/graphene hydrogel. Energy & Environmental Science. 2019, 12, 747-755.

[107] Tackett, B.M.; Gomez, E.; Chen, J.G. Net reduction of CO2 via its thermocatalytic and electrocatalytic transformation reactions in standard and hybrid processes. Nature Catalysis. 2019, 2, 381-386.

[108] Moioli, E.; Mutschler, R.; Züttel, A. Renewable energy storage via CO2 and H2 conversion to methane and methanol: assessment for small scale applications. Renewable and Sustainable Energy Reviews. 2019, 107, 497-506.

[109] Castellani, B.; Gambelli, A.M.; Morini, E.; Nastasi, B.; Presciutti, A.; Filipponi, M.; Nicolini, A.; Rossi, F. Experimental investigation on CO2 methanation process for solar energy storage compared to CO2-based methanol synthesis. Energies. 2017, 10, 855.

[110] Lee, W.J.; Li, C.; Prajitno, H.; Yoo, J.; Patel, J.; Yang, Y.; Lim, S. Recent trend in thermal catalytic low temperature CO2 methanation: A critical review. Catalysis today. 2021, 368, 2-19.

[111] Krammer, A.; Peham, M.; Lehner, M. 2D heterogeneous model of a polytropic methanation reactor. Journal of CO2 utilization. 2022, 62, 102059.

[112] Hu, F.; Chen, X.; Tu, Z.; Lu, Z.H.; Feng, G.; Zhang, R. Graphene aerogel supported Ni for CO2 hydrogenation to methane. Industrial & Engineering Chemistry Research. 2021, 60, 12235-12243.

[113] Deerattrakul, V.; Puengampholsrisook, P.; Limphirat, W.; Kongkachuichay, P. Characterization of supported Cu-Zn/graphene aerogel catalyst for direct CO2 hydrogenation to methanol: Effect of hydrothermal temperature on graphene aerogel synthesis. Catalysis Today. 2018, 314, 154-163.

[114] Deerattrakul, V.; Yigit, N.; Rupprechter, G.; Kongkachuichay, P. The roles of nitrogen species on graphene aerogel supported Cu-Zn as efficient catalysts for CO2 hydrogenation to methanol. Applied Catalysis A: General. 2019, 580, 46-52.